CONF-770131--1

PREPRINT UCRL-78911

Lawrence Livermore Laboratory

PHOTODISSOCIATION RATE CALCULATIONS

Frederick M. Luther
Donald J. Wuebbles

December 1976

This paper was prepared as a position paper for presentation at the NASA Workshop on CFM Assessment, January 10-14, 1977.

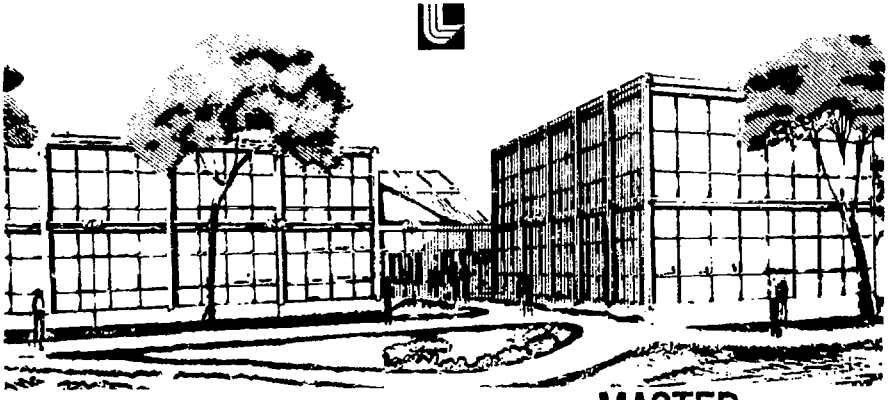

UCRL-78911

PHOTODISSOCIATION RATE CALCULATIONS*

Frederick M. Luther and Donald J. Wuebbles
Lawrence Livermore Laboratory, University of California,
Livermore, CA 94550

December 1976

INTRODUCTION

Stratospheric and tropospheric models that contain photochemically active species have almost universally invoked an assumption of pure absorption for computing solar fluxes and photodissociation rates. This has been due primarily to nothing more than limitations involving computer running time and capacity. For example, even with the simplest representations of atmospheric kinetics, models are often beset with computational constraints that normally lead to invoking the assumption of a purely absorbing atomic and molecular atmosphere for determining solar fluxes and the corresponding photodissociation rates. These limiting factors have been (and continue to be) sufficiently overriding that the roles of multiple scattering, the earth's surface reflection, clouds, and aerosols have remained a side issue in evaluating photochemical rates in atmospheric photochemical

*Work performed under the auspices of the U.S. Energy Research and Development Administration under contract No. W-7405-Eng-48 and supported in part by the High Altitude Pollution Program, U.S. Department of Transportation Federal Aviation Administration.

trace gas models; yet it is well-known that these factors can be significant in determining stratospheric and tropospheric radiative intensities at photodissociative wavelengths.

We will briefly review the approach used in pure molecular absorption calculations, and we will discuss the effect of including multiple scattering effects in a stratospheric model.

RADIATIVE TRANSFER FORMULATIONS IN ATMOSPHERIC PHOTOCHEMICAL MODELS

The solution of the one-dimensional purely absorbing source-free radiative transfer equation at a particular altitude z_p (km), solar zenith angle θ_o, and atmospheric composition $\{N_A(z)\}$ is given by

$$F_\lambda(z_p,\theta_o,\{N_A\},t) = F_\lambda(\infty)\exp[-\tau_\lambda(z_p,\theta_o,\{N_A\},t)] \qquad (1)$$

where $F_\lambda\, d\lambda$ is the flux of photons (in number per square centimeter per second) in the wavelength interval $d\lambda$ about λ. $F_\lambda(\infty)$ represents the solar flux at 1 AU, and the optical depth τ_λ is given by

$$\tau_\lambda(z_p,\theta_o,\{N_A\},t) \equiv \int_{z_p}^{\infty} dz \sum_A N_A(z,t)\,\sigma_T^A[\lambda,T(z)]\sec\theta_o(t) \qquad . \qquad (2)$$

In Eq. (2) the summation on A includes all atmospheric absorbers, each having number density $N_A(z,t)$ cm^{-3} and a total absorption cross section $\sigma_T^A[\lambda,T(z)]$ cm^2. Most generally, $\sigma_T^A[\lambda,T(z)]$ is a function of the temperature $T(z)$.

The photodissociation rate for transforming species i to species j is denoted by

$$J_{i\to j}(z_p,\theta_o,t)\ N_i(z_p,t)$$

where

$$J_{i\to j}(z_p,\theta_o,t) \equiv \int_{\text{all }\lambda} d\lambda\ \sigma_D^{\,i}[j,\lambda,T(z_p)]\ F_\lambda(z_p,\theta_o,\{N_A\},t) \quad . \quad (3)$$

The microscopic photodissociation cross section $\sigma_D^{\,i}[j,\lambda,T(z_p)]$ cm^2 is often written in terms of the so-called quantum yield $Q_\lambda(i\to j)$ as

$$\sigma_D^{\,i}[j,\lambda,T(z_p)] \equiv \sigma_T^{\,i}[\lambda,T(z_p)]\ Q_\lambda(i\to j) \quad . \quad (4)$$

Given microscopic cross-section data, $F_\lambda(\infty)$, $\{N_A(z)\}$, and θ_o, it is a straightforward matter to compute photodissociation coefficients.

It should be noted that uncertainties still remain in the data used to calculate the photodissociation coefficients in the models. For example, major uncertainties remain in the branching of O_3 photolysis near 310 nm to either $O(^3P)$ or $O(^1D)$, in the branching and quantum yield for NO_3 photolysis, and in the methodology for calculating the photolysis of species having banded or line absorption cross-section structures, such as O_2 or NO.

RADIATIVE TRANSFER CALCULATIONS INCLUDING MOLECULAR MULTIPLE SCATTERING AND SURFACE ALBEDO

When molecular multiple scattering and surface albedo are included in the radiative transfer calculation, (1) is no longer the solution of the radiative transfer equation. However, the flux in the direct solar beam

F_λ^S is given by an equation similar to (1):

$$F_\lambda^S(z_p,\theta_o,\{N_A\},t) = F_\lambda(\infty)\ \exp[-\tau_\lambda^S(z_p,\theta_o,\{N_A\},t)] \tag{5}$$

where the optical depth τ_λ^S along the slant path is given by

$$\tau_\lambda^S(z_p,\theta_o,\{N_A\},t)$$

$$\equiv \int_{z_p}^{\infty} dz \sum_A N_A(z,t)\ \sigma_T^A[\lambda,T(z)]\ \sec\theta_o(t)$$

$$+ \int_{z_p}^{\infty} dz \sum_i N_i(z,t)\ \sigma_R^i(\lambda)\ \sec\theta_o(t) \quad . \tag{6}$$

In (6) the summation on i includes all atmospheric species, and σ_R^i is the Rayleigh scattering cross section for species i. $F_\lambda^S(z_p,\theta_o,\{N_A\},t)$ differs from $F_\lambda(z_p,\theta_o,\{N_A\},t)$ as defined by (1) in that attenuation due to both absorption and scattering is included in (5), whereas only absorption is included in (1).

The photodissociation coefficient also depends upon the scattered (diffuse) radiation given by

$$J_{i\to j}(z_p,\theta_o,t) = \int_{\text{all }\lambda} d\lambda\ \sigma_D^i[j,\lambda,T(z_p)]$$

$$\cdot\left[F_\lambda^S(z_p,\theta_o,\{N_A\},t) + \int_{4\pi} I_\lambda(z_p,\omega)\ d\omega\right] \tag{7}$$

where I_λ is the specific intensity of the diffuse radiation and ω is a solid angle. Including the effect of molecular multiple scattering and surface albedo in the calculation is simply expressed by changing the value of F_λ appearing in (3). For clarity we define

$$F_\lambda^{MS}(\text{multiple scattering}) \equiv F_\lambda^S(z_p,\theta_o,\{N_A\},t) + \int_{4\pi} I_\lambda(z_p,\omega)\ d\omega \quad . \tag{8}$$

Henceforth, F_λ^{PA}(pure absorption) will refer to the flux defined by (1). Aside from substituting F_λ^{MS} in place of F_λ^{PA} in (3), all other aspects of the photodissociation rate calculation are the same as for the purely absorbing molecular atmosphere. Since $F_\lambda^{S}(z_p,\theta_o,\{N_A\},t)$ is less than F_λ^{PA}, F_λ^{MS} may be greater than or less than F_λ^{PA}, depending upon the intensity of the diffuse radiation.

MODEL DESCRIPTION

The effect of molecular scattering and surface albedo on ambient species concentrations and on model sensitivity has been assessed using a one-dimensional transport-kinetics model. The model has been described previously [Chang, 1975; Wuebbles and Chang, 1975], so only the main features of the model will be summarized.

The governing equation regarding the temporal variation in the number density of the i^{th} constituent c_i is given by the continuity equation,

$$\frac{\partial c_i}{\partial t} = P(c) - L(c)\, c_i - \frac{\partial}{\partial z}\left[K_z \rho \frac{\partial}{\partial z}\left(\frac{c_i}{\rho}\right)\right] \qquad (9)$$

where $P(c)$ is the production of c_i due to photochemical interactions of the other c_j species; $L(c)\, c_i$ is the loss of c_i due to chemical interaction of c_i with the other c_j species; K_z is the vertical transport coefficient; $\rho = \rho(z)$ is the ambient air density; and t and z are time and altitude, respectively.

The model atmosphere extends from the ground to 55 km and is divided into 44 layers. A total of 92 chemical (and photochemical) reactions are included in the model; 45 reactions describe O_x, NO_x, and HO_x chemistry,

and 47 reactions describe ClO_x chemistry. These reactions are used to dynamically describe the stratospheric vertical distributions of 20 minor atmospheric species ($O(^3P)$, O_3, NO, NO_2, N_2O, HNO_3, OH, HO_2, H_2O_2, Cl, $ClONO_2$, ClO, ClO_2, OClO, ClNO, $ClNO_2$, HCl, CCl_4, CF_2Cl_2 and $CFCl_3$). Three species (H, N, $O(^1D)$) are assumed to be in instantaneous equilibrium, and the vertical distributions of N_2, O_2, H_2O, CH_4 and H_2 are assumed constant throughout the calculations.

The vertical transport in the model is parameterized through the so-called "eddy" mixing coefficient K_z (see Wuebbles and Chang, 1975; Chang, 1975). The numerical technique, which is a variable order, multistep, implicit method, used to solve Equation (1), is that described by Chang et al. (1974). The boundary conditions are species dependent and are assumed to be either fixed or time varying source dependent concentrations at the surface and flux conditions at 55 km, the upper boundary.

The chemical reaction rates used in the model are shown in Table 1. Other reaction rates in the model are based on the review by Hampson and Garvin (1975). Detailed spectral data used in the calculations are as described by Gelinas (1974).

The effect of multiple scattering was incorporated into the photodissociation rate calculation by applying correction factors to the flux F_λ used in the pure absorption calculation (Eq. (1)). These correction factors, which are given by the ratio $F_\lambda^{MS}/F_\lambda^{PA}$, were computed for the unperturbed species profiles using a highly detailed solar radiation model (Luther and Gelinas, 1976). A separate factor was computed for each of the 44 levels and for each of the 148 wavelength intervals between 133 and 735 nm. Different sets of correction factors

were computed for each assumed value of surface albedo A_s using a solar zenith angle of 45°. The correction factors were assumed to be constant in the calculations.

Examples of correction factors for a solar zenith angle of 60° are shown in Figure 1 as functions of wavelength for selected altitudes and various values of A_s. Since no solar radiation reaches the earth's surface at wavelengths less than 290 nm, there is no dependence on surface albedo in this spectral region. The results for a surface albedo of zero demonstrate the effect of molecular multiple scattering alone, which is shown to have its maximum effect near 330 nm. The correction factors are nearly constant with height above 20 km, but they may vary significantly with height in the region below 20 km, which is where most scattering events occur. Correction factors for a solar zenith angle of 45° are somewhat larger than those shown for 60°, but they are qualitatively similar [Luther and Gelinas, 1976].

RESULTS

The effects of including multiple scattering in the photodissociation rate calculation may be of three types: (1) the effect on photodissociation coefficients, (2) the effect on ambient species concentration profiles, and (3) the effect on model sensitivity to perturbations.

1. Photodissociation Coefficients

As shown by Figure 1, the effect of multiple scattering should be largest for those species having strong absorption cross-sections at wavelengths greater than 300 nm. Table 2 compares photodissociation

coefficients for pure absorption and for multiple scattering computed for the ambient model atmosphere. Only those photodissociation reactions significantly affected by multiple scattering are shown in Table 2. In an attempt to account for the diurnal variation of photodissociation in the model, the solar flux was halved in these calculations.

The importance of the significant changes in reaction rate coefficients is reflected in the species concentration profiles and in the model sensitivity.

2. Species Concentration Profiles

The concentration profiles for selected O_x, HO_x, NO_x, and ClX species are shown in Figures 2-5 for the ambient atmosphere prior to inclusion of multiple scattering and prior to the release of CFM's. These figures are included in order to define the reference conditions for assessing the fractional change in concentration caused by multiple scattering.

The changes in concentration of chemical species due to multiple scattering relative to the pure absorption calculation were computed for cases with and without $ClONO_2$. Inclusion of $ClONO_2$ significantly affected the results for the chlorine containing species, but it had a small effect on the other species (< 5% change in NO_2 and much less for other species). The following figures correspond to the case including $ClONO_2$ and with $A_s = 0.25$ unless otherwise specified.

The effect of multiple scattering on O_x species is shown in Figure 6. The large percentage increase in $O(^1D)$ near 10 km occurs where the ambient concentration is very small; nevertheless, it is significant in terms of stratospheric chemistry. The increases in $O(^3P)$ and $O(^1D)$ in the region 20-30 km are due to increased photolysis of O_3. Because of differences in ambient concentrations, a small percentage decrease in O_3 causes large percentage increases in the other species. The increase in $O(^3P)$ near 40 km is due

primarily to increased photolysis of NO_2. The increase in O_3 at this height occurs because the chemical production of O_3 by $O + O_2$ is increased more than the photolysis of O_3.

Figure 7 shows the effect of multiple scattering on HO_x species. The increase in OH results from $HNO_3 \xrightarrow{h\nu} OH + NO_2$ and $H_2O_2 \xrightarrow{h\nu} 2OH$. The peak concentration in H_2O_2 occurs near 28 km, so a small percentage decrease in H_2O_2 in this region can cause a large percentage increase in OH. The increase in HO_2 is chemically linked to the increase in OH.

Figure 8 shows the effect of multiple scattering on NO_x species. There is a very large increase in NO near 20 km due to increased photolysis of NO_2. NO_2 increases because of increased photolysis of HNO_3. There is very little HNO_3 above 30 km, so NO_2 decreases in this region because it is essentially the only source of NO.

The effect of multiple scattering on $ClONO_2$ is shown in Figure 9. The concentration is reduced 20-40% between 20 and 30 km, which is the region of maximum $ClONO_2$ concentration. Photolysis of $ClONO_2$ affects several other chlorine containing species through a complex chain of reactions. Certain key reactions are:

$$ClONO_2 \xrightarrow{h\nu} ClO + NO_2$$

$$ClO + NO \rightarrow Cl + NO_2$$

$$Cl + CH_4 \rightarrow HCl + CH_3$$

The peak concentration of $ClONO_2$ occurs near 25 km, so photolysis of $ClONO_2$ acts as a strong source of ClO in this region. The large increase in NO between 20-30 km tends to destroy ClO, leading to a net decrease in ClO in this region (Figure 10) and an increase in Cl (Figure 11). The increase in

Cl leads to an increase in HCl (Figure 12) through reaction with CH_4. These results also indicate that inclusion of $ClONO_2$ has a more significant effect on ClX species than the choice of surface albedo.

Ratios of total column abundances computed with multiple scattering to that with pure absorption were 0.94 (O_3), 0.975 (NO_2) and 1.21 (NO).

The above analysis is overly simplified considering the complexity and interaction of the various chemical cycles. Nevertheless, we have attempted to summarize the major mechanisms by which multiple scattering affects species concentrations.

3. Model Sensitivity

Model sensitivity was tested for two types of perturbations: release of CFM's at constant production levels and the stratospheric injection of NO_x. In each case calculations were made with and without $ClONO_2$. The CFM calculation to steady state assumes that $CFCl_3$ and CF_2Cl_2 are released at 1973 rates as estimated by McCarthy (1974). The ozone reductions computed at steady state are shown in Table 3 for the various cases.

Multiple scattering significantly reduces the sensitivity of the model without $ClONO_2$. The ozone reduction changed from -15.28% to -12.45% when multiple scattering was included with $A_s = 0.25$.

The model with $ClONO_2$ is the more complete model according to our present understanding. When multiple scattering is included in this model, there is a negligible change in model sensitivity for $A_s = 0.25$ in spite of significant changes in photodissociation rates and species concentrations. The decrease in sensitivity for the model without $ClONO_2$ occurs because multiple scattering shifts the balance between NO_2 and NO

toward NO. This increases the importance of the reaction ClO + NO relative to ClO + O, thus decreasing the effectiveness of the chlorine catalytic cycle. The effect of including $ClONO_2$ is also reduced by multiple scattering. This occurs primarily because of increased $ClONO_2$ photolysis reducing the $ClONO_2$ concentration. Thus, while the O_3 destructiveness of the ClO_x catalytic cycle is reduced by multiple scattering, the ameliorating effect of $ClONO_2$ is also reduced. The net effect is that the CFM calculations including $ClONO_2$ with and without multiple scattering give approximately the same reduction in ozone. The model sensitivity depends upon the choice of A_s, as indicated by the reduced model sensitivity for $A_s = 0.75$.

Model sensitivity to stratospheric injections of NO_x is shown in Table 4. For these calculations, NO_x was injected globally at a rate of 2.5×10^9 kg/yr as NO_2 uniformly distributed over a 1-km thick shell centered at either 17 or 20 km altitude. Multiple scattering significantly increased the sensitivity of the model without $ClONO_2$, but it had only a small effect (<5%) on the sensitivity of the model with $ClONO_2$.

DISCUSSION

The results above provide a partial assessment of effect of including multiple scattering in the photodissociation rate calculation of transport-kinetics models. Multiple scattering significantly affects photodissociation rates, particularly at wavelengths greater than 290 nm, and this is reflected in the species concentration profiles. The degree to which multiple scattering affects model sensitivity to various perturbations depends upon model chemistry, solar zenith angle, and surface albedo. The assessment has not yet been extended to diurnal or two-dimensional calculations.

REFERENCES

Chang, J.S., A. C. Hindmarsh, and N. K. Madsen, Simulation of Chemical Kinetics Transport in the Stratosphere, Stiff Differential Systems, Ed. R. A. Willoughby, Plenum Publishing Corporation, New York, 51-65, 1974.

Chang, J. S., Effect, on Ozone of Trace Gases from Propulsion Effluents in the Stratosphere, The Stratosphere Perturbed by Propulsion Effluents (CIAP Monograph 3), Report DOT-TST-75-53, Chapter 5, U.S. Department of Transportation, Washington, D.C., 1975.

Hampson, R. F., and D. Garvin (Eds.), Chemical Kinetic and Photochemical Data for Modeling Atmospheric Chemistry, NBS Technical Note 866, National Bureau of Standards, Gaithersburg, MD, 1975.

Luther, F. M. and R. J. Gelinas, Effect of Molecular Multiple Scattering and Surface Albedo on Atmospheric Photodissociation Rates, J. Geophys. Res., 81, 1125-1132, 1976.

McCarthy, R. L., Fluorocarbons in the Environment, paper presented at the American Geophysical Union Meeting, San Francisco, CA, Dec. 13, 1974.

Wuebbles, D. J., and J. S. Chang, Sensitivity of Time-Varying Parameters in Stratospheric Modeling, J. Geophys. Res., 80, 2637-2642, 1975.

TABLE 1

1976 Chemistry: O_x, NO_x and HO_x Chemistry

Reaction	Rate
$O_2 + h\nu \rightarrow O + O$	QJ(1)
$O_3 + h\nu \rightarrow O + O_2$	QJ(2)
$O_3 + h\nu \rightarrow O(^1D) + O_2$	QJ(3)
$O + O_2 + M \rightarrow O_3 + M$	1.07×10^{-34} exp(510/T)
$O + O_3 \rightarrow 2O_2$	1.9×10^{-11} exp(-2300/T)
$NO_2 + h\nu \rightarrow NO + O$	QJ(4)
$O_3 + NO \rightarrow NO_2 + O_2$	9.0×10^{-13}exp(-1200/T)
$O + NO_2 \rightarrow NO + O_2$	9.1×10^{-12}
$N_2O + h\nu \rightarrow N_2 + O(^1D)$	QJ(5)
$N_2O + O(^1D) \rightarrow N_2 + O_2$	7×10^{-11}
$N_2O + O(^1D) \rightarrow 2NO$	7×10^{-11}
$NO + h\nu \rightarrow N + O$	QJ(6)
$N + O_2 \rightarrow NO + O$	1.1×10^{-14} T exp(-3150/T)
$N + NO \rightarrow N_2 + O$	2.7×10^{-11}
$O(^1D) + H_2O \rightarrow 2OH$	2.1×10^{-10}
$O(^1D) + CH_4 \rightarrow OH + CH_3$	1.3×10^{-10}
$HNO_3 + h\nu \rightarrow OH + NO_2$	QJ(7)
$O_3 + OH \rightarrow HO_2 + C_2$	1.6×10^{-12} exp(-1000/T)
$O + OH \rightarrow O_2 + H$	4.2×10^{-11}
$O_3 + HO_2 \rightarrow OH + 2O_2$	1.0×10^{-13} exp(-1250/T)
$O + HO_2 \rightarrow OH + O_2$	3×10^{-11}
$H + O_2 + M \rightarrow HO_2 + M$	2.08×10^{-32} exp(290/T)
$O_3 + H \rightarrow OH + O_2$	1.23×10^{-10} exp(-562/T)

TABLE 1 1976 CHEM CONT

Reaction	Rate
$HO_2 + HO_2 \rightarrow H_2O_2 + O_2$	$1.7 \times 10^{-11} \exp(-500/T)$
$HO_2 + OH \rightarrow H_2O + O_2$	2.0×10^{-11}
$OH + NO_2 + M \rightarrow HNO_3 + M$	$\frac{2.76 \times 10^{-13} \exp(880/T)}{1.166 \times 10^{18} \exp(222/T) + M}$
$OH + HNO_3 \rightarrow H_2O + NO_3$	8.9×10^{-14}
$H_2O_2 + h\nu \rightarrow 2OH$	QJ(8)
$H_2O_2 + OH \rightarrow H_2O + HO_2$	$1.7 \times 10^{-11} \exp(-910/T)$
$N_2 + O(^1D) + M \rightarrow N_2O + M$	2.8×10^{-36}
$N + NO_2 \rightarrow N_2O + O$	1.4×10^{-12}
$NO + O + M \rightarrow NO_2 + M$	$3.96 \times 10^{-33} \exp(940/T)$
$NO + HO_2 \rightarrow NO_2 + OH$	2.0×10^{-13}
$H_2 + O(^1D) \rightarrow OH + H$	2.9×10^{-10}
$OH + OH \rightarrow H_2O + O$	$1.0 \times 10^{-11} \exp(-550/T)$
$N + O_3 \rightarrow NO + O_2$	5.7×10^{-13}
$NO_2 + O_3 \rightarrow NO_3 + O_2$	$1.2 \times 10^{-13} \exp(-2450/T)$
$HO_2 + h\nu \rightarrow OH + O$	QJ(9)
$OH + CH_4 \rightarrow H_2O + CH_3$	$2.36 \times 10^{-12} \exp(-1710/T)$
$OH + OH + M \rightarrow H_2O_2 + M$	$2.5 \times 10^{-33} \exp(2500/T)$
$H_2O_2 + O \rightarrow OH + HO_2$	$2.75 \times 10^{-12} \exp(-2125/T)$
$O + CH_4 \rightarrow OH + CH_3$	$3.5 \times 10^{-11} \exp(-4550/T)$
$CO + OH \rightarrow H + CO_2$	1.4×10^{-13}
$O(^1D) + M \rightarrow O + M$	$2.2 \times 10^{-11} \exp(92/T)$
$NO_3 + h\nu \rightarrow NO_2 + O$	0.66
$\rightarrow NO + O_2$	0.34

TABLE 1 1976 CHEM CONT

ClO_x Chemistry

Reaction	Rate
$Cl + O_3 \rightarrow ClO + O_2$	$2.97 \times 10^{-11} \exp(-243/T)$
$Cl + OClO \rightarrow 2ClO$	5.9×10^{-11}
$Cl + O_2 + M \rightarrow ClO_2 + M$	$1.7 \times 10^{-33}(\frac{300}{T})$
$Cl + CH_4 \rightarrow HCl + CH_3$	$5.4 \times 10^{-12} \exp(-1133/T)$
$Cl + ClO_2 \rightarrow Cl_2 + O_2$	5×10^{-11}
$Cl + ClO_2 \rightarrow 2ClO$	1.4×10^{-12}
$Cl + NO + M \rightarrow ClNO + M$	$1.7 \times 10^{-32} \exp(553/T)$
$Cl + ClNO \rightarrow Cl_2 + NO$	3.0×10^{-11}
$Cl + NO_2 + M \rightarrow ClNO_2 + M$	$6.9 \times 10^{-34} \exp(2115/T)$
$Cl + ClNO_2 \rightarrow Cl_2 + NO_2$	3.0×10^{-12}
$ClO + O \rightarrow Cl + O_2$	$3.38 \times 10^{-11} \exp(+75/T)$
$NO + ClO \rightarrow NO_2 + Cl$	$1.13 \times 10^{-11} \exp(+200/T)$
$ClO + O_3 \rightarrow ClO_2 + O_2$	$1.0 \times 10^{-12} \exp(-2763/T)$
$ClO + O_3 \rightarrow OClO + O_2$	$1.0 \times 10^{-12} \exp(-2763/T)$
$ClO + NO_2 \xrightarrow{M} ClNO_3$	$0.05*HNO_3$ formation (incl. diurnal effect)
$ClO + ClO \rightarrow Cl + OClO$	$2.0 \times 10^{-12} \exp(-2300/T)$
$ClO + ClO \rightarrow Cl_2 + O_2$	$2.0 \times 10^{-13} \exp(-1260/T)$
$ClO + ClO \rightarrow Cl + ClO_2$	$2 \times 10^{-13} \exp(-1260/T)$
$HCl + O(^1D) \rightarrow Cl + OH$	2×10^{-10}
$ClNO_3 + HCl \rightarrow O_2 + HNO_3$	0.0
$OH + HCl \rightarrow H_2O + Cl$	$2.0 \times 10^{-12} \exp(-310/T)$
$O + HCl \rightarrow OH + Cl$	$1.75 \times 10^{-12} \exp(-2273/T)$
$ClO_2 + M \rightarrow Cl + O_2 + M$	$1.5 \times 10^{-8} \exp(-4000/T)$
$O + OClO \rightarrow ClO + O_2$	5.0×10^{-13}

TABLE 1 1976 CHEM CONT

ClO_x Chemistry

Reaction	Rate
$NO + OClO \rightarrow NO_2 + ClO$	3.4×10^{-13}
$N + OClO \rightarrow NO + ClO$	6.0×10^{-13}
$H + OClO \rightarrow OH + ClO$	5.7×10^{-11}
$Cl + OH \rightarrow HCl + O$	2.0×10^{-12} exp(-1878/T)
$Cl + HO_2 \rightarrow HCl + O_2$	3.0×10^{-11}
$Cl + HNO_3 \rightarrow HCl + NO_3$	4.0×10^{-12} exp(-1500/T)
$ClO_2 + HO_2 \rightarrow HCl + 2O_2$	3.0×10^{-12}
$Cl_2 + h\nu \rightarrow 2Cl$	QCJ(1)
$HCl + h\nu \rightarrow H + Cl$	QCJ(2)
$ClO_2 + h\nu \rightarrow ClO + O(^1D)$	QCJ(3)
$ClO + h\nu \rightarrow Cl + O$	QCJ(4)
$ClO + h\nu \rightarrow Cl + O(^1D)$	QCJ(5)
$ClNO + h\nu \rightarrow Cl + NO$	QCJ(6)
$ClNO_2 + h\nu \rightarrow Cl + NO_2$	QCJ(7)
$OClO + h\nu \rightarrow ClO + O(^1D)$	QCJ(8)
$OClO + h\nu \rightarrow ClO + O$	QCJ(9)
$CF_2Cl_2 + h\nu \rightarrow 2Cl$	QCJ(10)
$CFCl_3 + h\nu \rightarrow 2.5\ Cl$	QCJ(11)
$CCl_4 + h\nu \rightarrow 2Cl$	QCJ(12)
$CFCl_3 + O(^1D) \rightarrow 2Cl$	5.8×10^{-10}
$CF_2Cl_2 + O(^1D) \rightarrow 2Cl$	5.3×10^{-10}
$Cl + H_2 \rightarrow HCl + H$	5.7×10^{-11} exp(-2400/T)
$Cl + H_2O_2 \rightarrow HCl + HO_2$	1.0×10^{-11} exp(-810/T)
$O + ClNO_3 \rightarrow ClO + NO_3$	2.1×10^{-13}
$OH + CH_3Cl \rightarrow H_2O + HO_2 + HCl$	1.58×10^{-12} exp(-1049/T)

TABLE 2

COMPARISON OF PHOTODISSOCIATION RATES
CALCULATED WITH AND WITHOUT MULTIPLE SCATTERING

Altitude, km	J_{PA}	J_{MS}	J_{MS}/J_{PA}
$O_3 + h\nu \rightarrow O(^3P) + O_2$			
10	2.02×10^{-4}	3.01×10^{-4}	1.49
20	2.07	3.00	1.45
30	2.41	3.21	1.33
40	2.74	3.49	1.27
$O_3 + h\nu \rightarrow O(^1D) + O_2$			
10	5.83×10^{-6}	1.08×10^{-5}	1.85
20	7.97×10^{-6}	1.22×10^{-5}	1.53
30	5.78×10^{-5}	6.27×10^{-5}	1.08
40	9.32×10^{-4}	9.14×10^{-4}	0.98
$NO_2 + h\nu \rightarrow NO + O$			
10	4.72	7.77×10^{-3}	1.65
20	4.74	7.76	1.64
30	4.85	7.68	1.58
40	4.97	7.73	1.56
$HNO_3 + h\nu \rightarrow OH + NO_2$			
10	2.72×10^{-7}	4.82×10^{-7}	1.77
20	3.37×10^{-7}	5.18×10^{-7}	1.54
30	4.98×10^{-6}	5.11×10^{-6}	1.03
40	3.52×10^{-5}	3.52×10^{-5}	1.00

TABLE 2 CONT

Altitude, km	J_{PA}	J_{MS}	J_{MS}/J_{PA}
$H_2O_2 + h\nu \rightarrow 2OH$			
10	1.90×10^{-6}	3.35×10^{-6}	1.76
20	2.23×10^{-6}	3.46×10^{-6}	1.55
30	6.57×10^{-6}	7.29×10^{-6}	1.11
40	3.51×10^{-5}	3.52×10^{-5}	1.00
$ClO + h\nu \rightarrow Cl + O$			
10	1.72×10^{-5}	3.25×10^{-5}	1.89
20	2.55×10^{-5}	3.82×10^{-5}	1.50
30	1.92×10^{-4}	2.05×10^{-4}	1.07
40	1.64×10^{-3}	1.62×10^{-3}	0.99
$ClONO_2 + h\nu \rightarrow ClO + NO_2$			
10	3.31×10^{-5}	5.57×10^{-5}	1.68
20	3.43×10^{-5}	5.61×10^{-5}	1.64
30	5.22×10^{-5}	7.07×10^{-5}	1.35
40	2.24×10^{-4}	2.38×10^{-4}	1.06

TABLE 3

CHANGE IN THE OZONE COLUMN DUE TO THE ATMOSPHERIC RELEASE OF CFM'S -- STEADY STATE VALUE AT CONSTANT PRODUCTION

CASE	CHANGE IN OZONE COLUMN - %		
	WITHOUT MULTIPLE SCATTERING	WITH MULTIPLE SCATTERING	RATIO
		$A_S = 0.25$	
WITHOUT $ClONO_2$	-15.28	-12.45	0.81
WITH $ClONO_2$	-8.97	-9.03	1.01
		$A_S = 0.75$	
WITH $ClONO_2$	-8.97	-6.91	0.77

TABLE 4

NO_x INJECTION

2.5×10^9 KG/YR AS NO_2

CASE	CHANGE IN OZONE COLUMN - %		
	WITHOUT MULTIPLE SCATTERING	MULTIPLE SCATTERING $A_S = 0.25$	RATIO
17-KM INJECTION:			
WITHOUT $ClONO_2$	-0.75	-0.97	1.29
WITH $ClONO_2$	-1.07	-1.10	1.03
20-KM INJECTION:			
WITHOUT $ClONO_2$	-3.23	-3.82	1.18
WITH $ClONO_2$	-3.93	-4.12	1.05

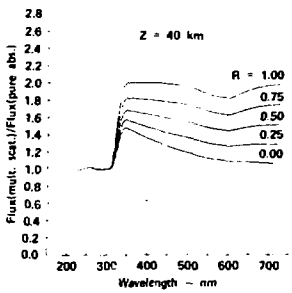

Fig. 1*a*

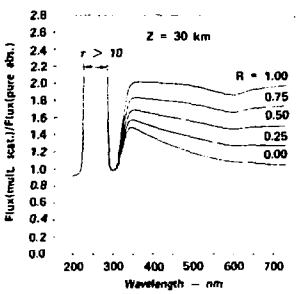

Fig. 1*b*

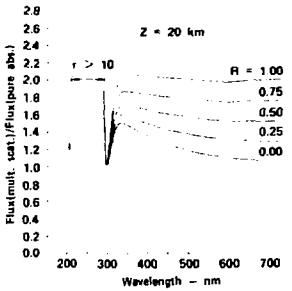

Fig. 1*c*

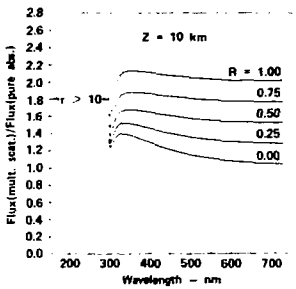

Fig. 1*d*

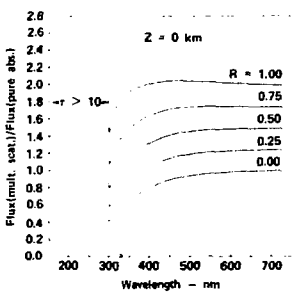

Fig. 1*e*

Fig. 1. Flux ratio versus wavelength for a solar zenith angle of 60° and selected values of surface albedo R at altitudes z of (*a*) 40 km, (*b*) 30 km, (*c*) 20 km, (*d*) 10 km, and (*e*) 0 km.

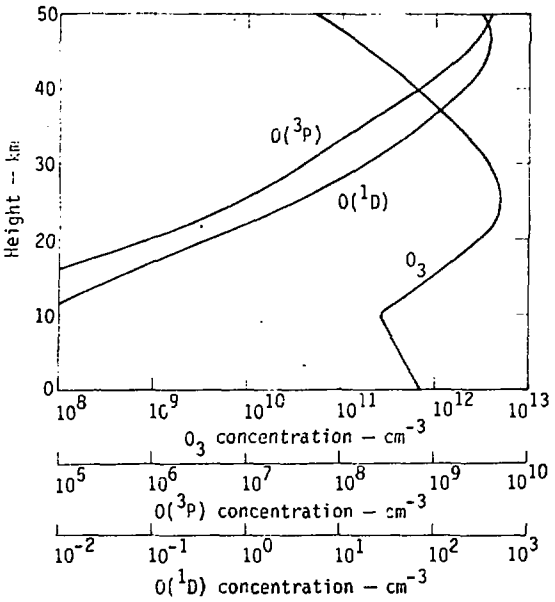

Fig. 2. Ambient concentration profiles of O_3, $O(^3P)$, and $O(^1D)$.

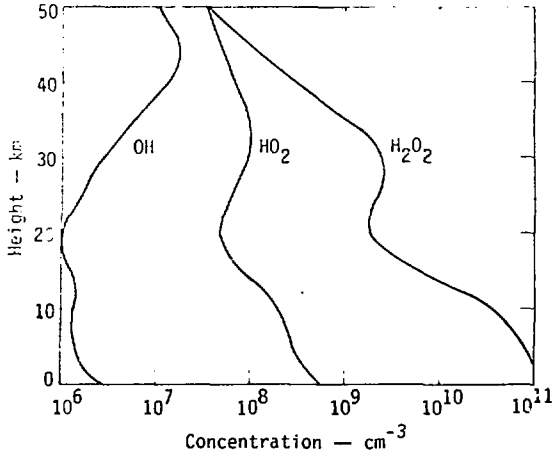

Fig. 3. Ambient concentration profiles of OH, HO_2, and H_2O_2.

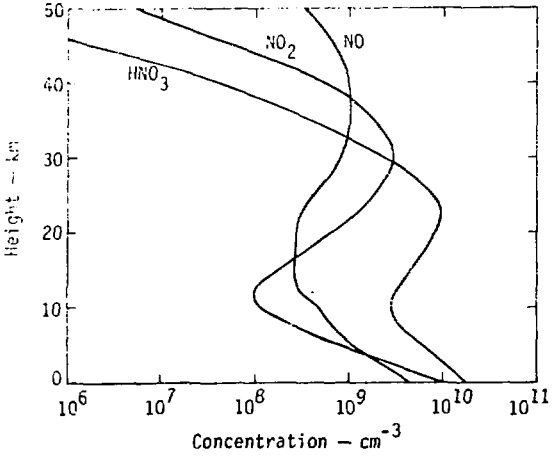

Fig. 4. Ambient concentration profiles of NO_2, NO, and HNO_3.

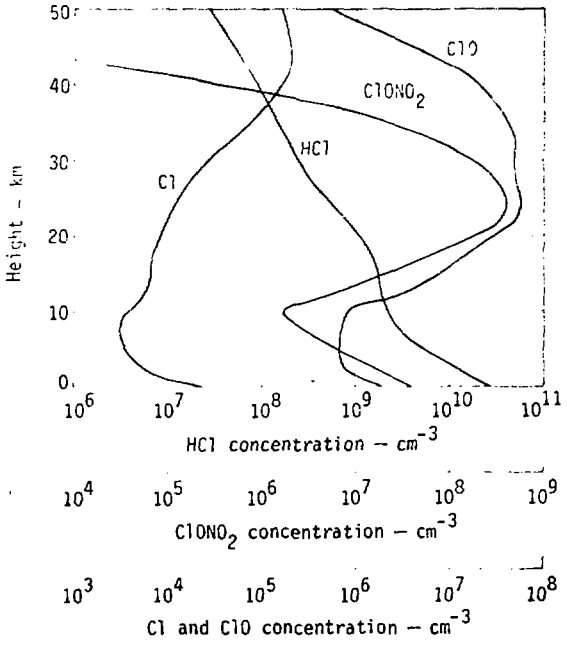

Fig. 5. Ambient concentration profiles of species containing chlorine.

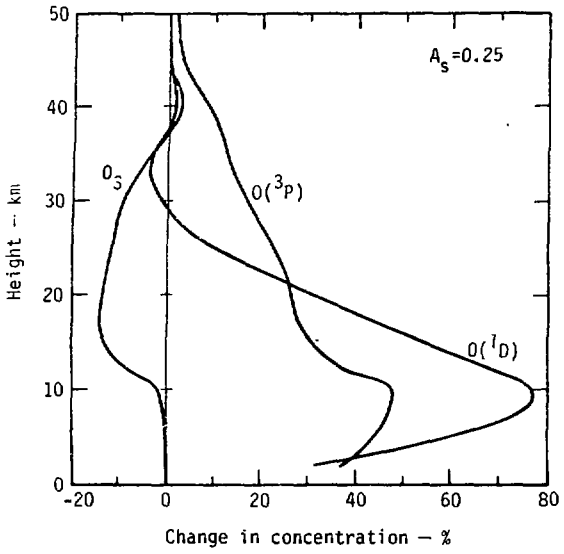

Fig. 6. The change in O_x species concentrations due to multiple scattering with A_s = 0.25.

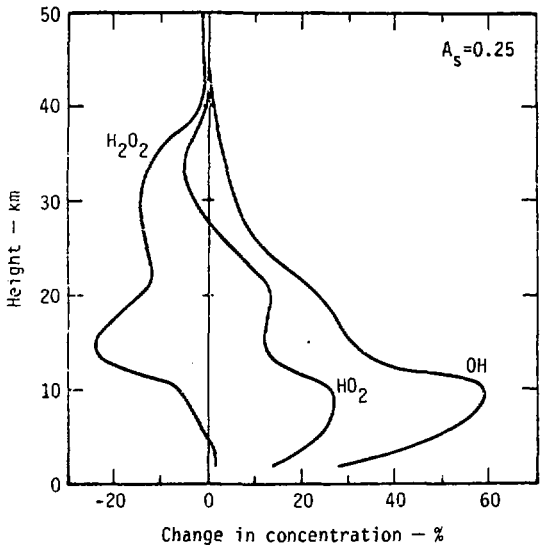

Fig. 7. The change in HO_x species concentrations due to multiple scattering with A_s = 0.25.

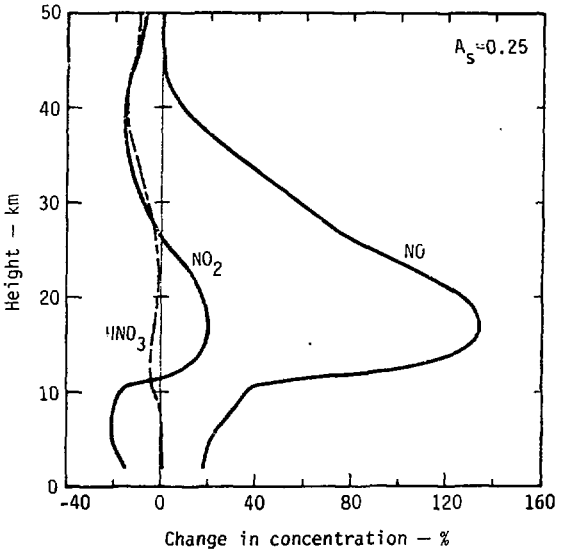

Fig. 8. The change in NO_x species concentrations due to multiple scattering with A_s = 0.25.

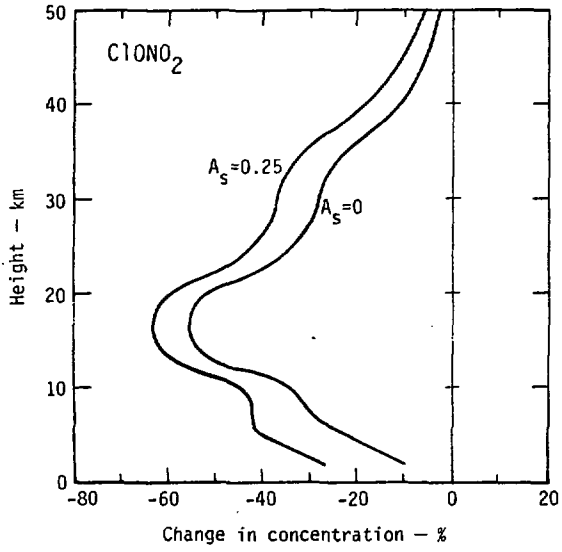

Fig. 9. The change in concentration of $ClONO_2$ due to multiple scattering for A_s = 0 and 0.25.

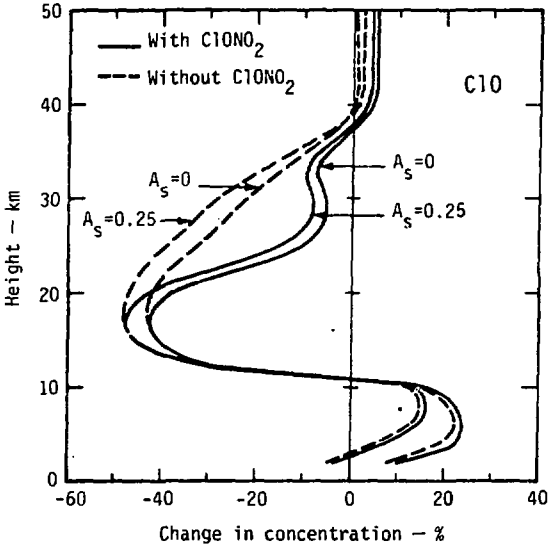

Fig. 10. The change in concentration of ClO due to multiple scattering.

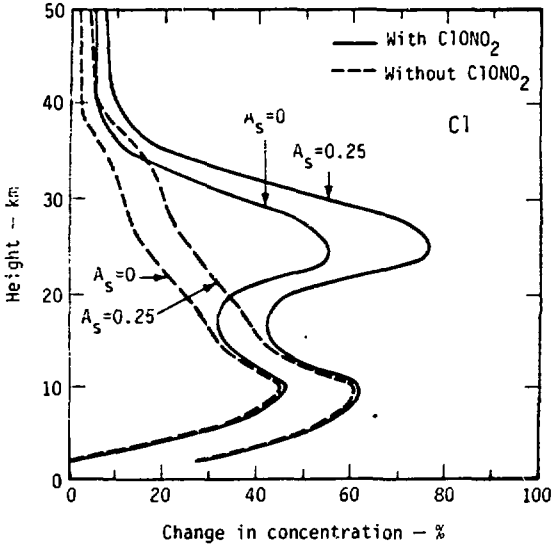

Fig. 11. The change in concentration of Cl due to multiple scattering.

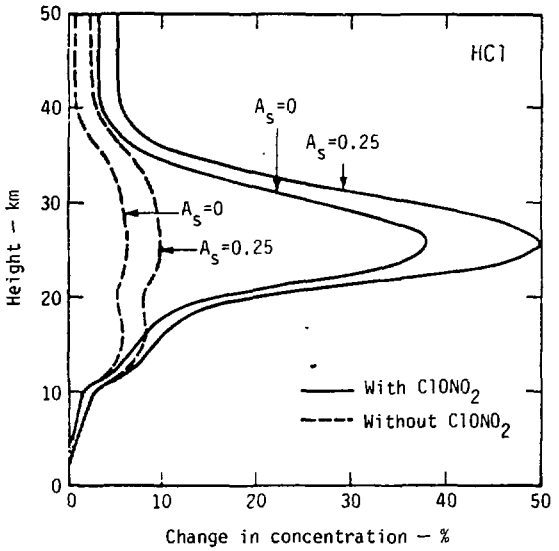

Fig. 12. The change in concentration of HCl due to multiple scattering.